Submission code: Y6DGK48R9A

See this and other abstracts on our website: https://home.sbgf.org.br/Pages/resumos.php

Monitoring CO2 Plumes with MCSEM in Anisotropic Media.

Jhonattas Barros (Universidade Federal do Pará), Marcos Silva (Universidade Federal do Pará), Jéssica Itó (Universidade Federal do Pará)

Monitoring CO_2 Plumes with MCSEM in Anisotropic Media.

Abstract Summary

The Marine Controlled Source Electromagnetic (MCSEM) method has proven to be highly effective in detecting high-resistivity zones in the subsurface. In this study, we simulate two 3D CO_2 reservoir models to analyze how MCSEM response curves behave in the presence of anisotropic plumes. We also investigate the temporal evolution and lateral migration of these plumes at different frequencies. Numerical modeling was performed using the vector finite element method, and electromagnetic responses, such as electric field amplitudes, were processed and visualized using MATLAB.

Introduction

The increasing atmospheric CO_2 concentrations have significantly accelerated global warming, highlighting the urgent need for effective carbon sequestration solutions in geological formations Soeder (2021); Zhang et al. (2023). This study investigates the application of the Marine Controlled-Source Electromagnetic (MCSEM) method for monitoring CO_2 plumes, capitalizing on its sensitivity to subsurface resistivity variations to track injected CO_2 in deep reservoirs Kang et al. (2015).

Through vector finite element modeling, we systematically analyze the plume's temporal evolution and lateral displacement across multiple frequencies (0.5–2 Hz), enabling the generation of detailed anomaly maps that visualize spatial distribution patterns over time. Complementing this approach, numerical modeling techniques are employed to predict post-injection plume migration dynamics, providing critical insights for reservoir management SOUZA et al. (2007). The research focuses on a broadside acquisition scheme with 55 strategically positioned transmitters, evaluating plume detection capabilities in a representative 4-layer marine model (seawater: 0.3 Ωm, sediment: 1 Ωm, trap: 5 Ωm) containing five distinct plume levels.

Methodology

The Marine Controlled Source Electromagnetic (MCSEM) method is highly effective in detecting resistive targets in the marine subsurface due to its sensitivity to resistivity variations. In CO_2-saturated environments, it enables the detection and characterization of plumes through the analysis of reflected signals Fawad and Mondol (2021). According to REZENDE et al. (2011), MCSEM surveys involve the deployment of seafloor receivers (Rx) while a vessel tows a horizontal electric dipole (HED) near the seabed. The HED emits electromagnetic waves that propagate through the subsurface and are partially reflected at resistivity contrasts, being recorded by the receivers.

Marine substrates and subsurface formations often exhibit **electric anisotropy**, meaning that resistivity varies with direction (both vertically and horizontally). A TIV (Transversely Isotropic Vertical) anisotropy was adopted, in which resistivity is constant in the horizontal plane but varies in the vertical direction. This anisotropy significantly affects data responses, particularly in *broadside* acquisition geometries, where transmitters and receivers are not aligned. In such cases, the receivers are arranged in a grid, which enhances anisotropic effects in the interpretation of the data Wang et al. (2018). Numerical modeling was performed using the *vector finite element method*, which discretizes the domain with tetrahedral elements and solves the electromagnetic problem along their edges. This approach provides greater accuracy in representing electric and magnetic fields, especially in anisotropic media Xiong et al. (2023).

Results

Two synthetic models were developed to illustrate the influence of CO_2 plume migration on MCSEM responses, considering a broadside acquisition geometry. Both models share the same structural configuration, composed of four layers: a water column (1 km, 0.3 Ω·m), a sediment layer (1 km, 1 Ω·m), a trap-like rock formation (0.4 km, 5 Ω·m) and a lower sediment layer (1 Ω·m) that extends into the half-space. The main difference between the models lies in the migration path of the CO_2 plume. In Model 1, the plume migrates vertically along the y-axis in a symmetric manner. In Model 2, the plume also migrates vertically but with a progressive lateral shift to the right.

In both models, plume monitoring was simulated in five stages, representing different times after injection. Initially, the plume has a thickness of 50 m, a diameter of 1 km, and anisotropic resistivities of 90 Ω·m in the x-direction and 120 Ω·m in the y-direction, located at a depth of 1.3 km below the seafloor. As the stages progress, the plume expands laterally and varies in depth. In Model 1, this expansion occurs symmetrically, whereas in Model 2, the center of the plume changes laterally from 0.5 km (stage 1) to 4 km (stage 5) to the right. Figure 1a) shows the evolution in Model 1, and Figure 1b) in Model 2.

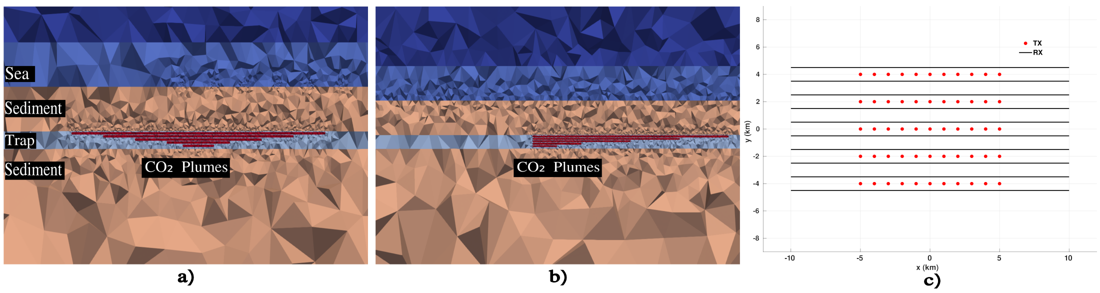

Figure 1: Homogeneous and Anisotropic Marine Model with 4 layers (Seawater - 0.3 Ωm, Sediment - 1 Ωm, Trap - 5 Ωm, and Sediment - 1 Ωm) showing the 5 plume levels within the rock formation.

The adopted data acquisition scheme was of the broadside type, with transmitters oriented differently from the measurement lines. This setup was used in both models, consisting of 10 lines of measurement points and 5 lines of receivers, each with 11 receivers, totaling 55 receivers across the seabed (see Figure 1c). Data were collected at four frequencies—0.5 Hz, 0.75 Hz, 1 Hz, and 2 Hz—to determine which best captured the plume's growth and migration. To present the results, one representative receiver was selected per model: -5 km on line 3 for Model 1, and -1 km on line 3 for Model 2.

Figure 2 displays the electric field amplitude at 2 Hz, the optimal frequency for both models. The analysis considers the plume's effect across five growth stages, showing a progressively stronger impact on the electric field as the plume evolves.

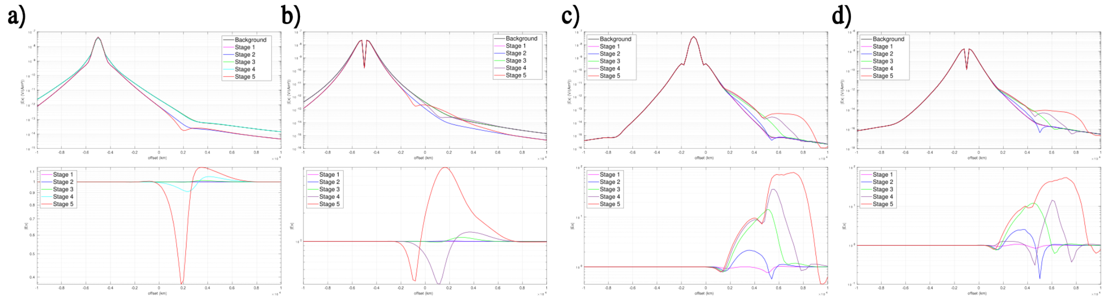

Figure 2: The CO_2 plume at 2 Hz displays the electric fields in x- (a) and y-directions (b), with normalizations below, measured by the transmitter at -5 km in Model 1. Figures (c) and (d) show the same fields measured at the receiver in -1 km in Model 2.

In figures a) and b), for Model 1, the plume expands symmetrically along the y-axis toward the surface, increasing in diameter. This symmetrical behavior is most evident in the y-direction field (b), which, due to model anisotropy, highlights the plume's influence more clearly.

In contrast, figures c) and d), for Model 2, show not only vertical growth but also lateral migration to the right, creating asymmetry relative to the y-axis. Consequently, the MCSEM response displays stronger contrasts in the x-direction, reflecting both the plume's asymmetrical path and the anisotropic nature of the model.

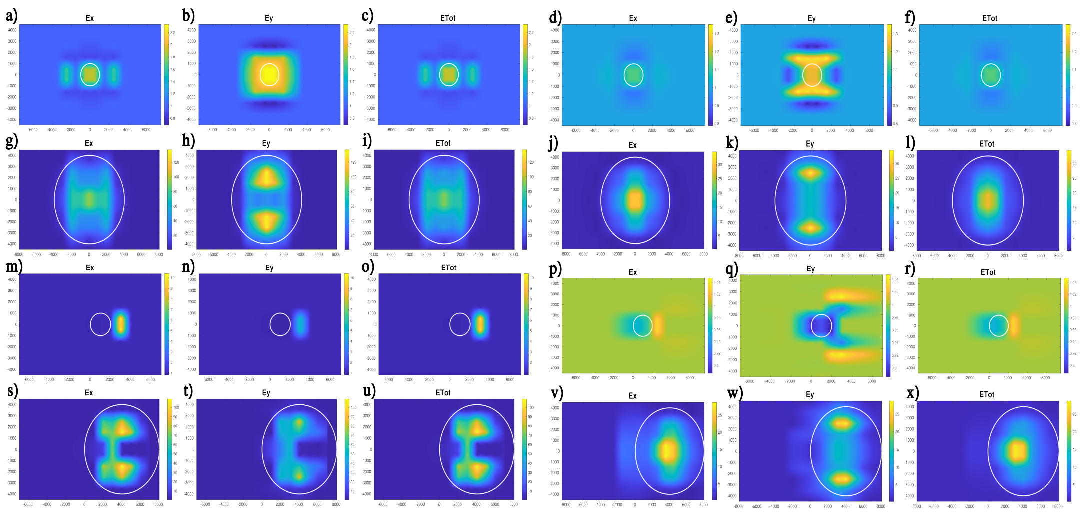

Figure 3: Anomaly maps generated over the complete acquisition grid for two distinct models, each evaluated at two stages (Stage 2 and Stage 5) and at two frequencies (2 Hz and 0.75 Hz). Subfigures a) to l) correspond to Model 1, where a), b), and c) represent Stage 2 at 2 Hz; d), e), and f) represent Stage 2 at 0.75 Hz; g), h), and i) represent Stage 5 at 2 Hz; and j), k), and l) represent Stage 5 at 0.75 Hz. Subfigures m) to x) correspond to Model 2, with m), n), and o) representing Stage 2 at 2 Hz; p), q), and r) representing Stage 2 at 0.75 Hz; s), t), and u) representing Stage 5 at 2 Hz; and v), w), and x) representing Stage 5 at 0.75 Hz. Each set of three images shows the electric field components in the Ex and Ey directions, followed by the total electric field (ETot).

In Figure 3, you can see a broader view of the entire acquisition grid, where various anomaly maps were generated. Figure 3 shows two different models. From a) to l), we have Model 1, divided into two stages and two frequencies. Stage 2 is shown in figures a), b) and c) for the 2 Hz frequency, and in figures d), e) and f) for the 0.75 Hz frequency. Stage 5 is shown in figures g), h) and i) for the frequency of 2 Hz, and in figures j), k) and l) for the frequency of 0.75 Hz.

In Figure 3, we also have model 2 from m) to x), divided into two stages and two frequencies. Stage 2 is represented in figures m), n) and o) for the frequency of 2 Hz, and in figures p), q) and r) for the frequency of 0.75 Hz. Stage 5 is shown in figures s), t) and u) for the frequency of 2 Hz, and in figures v), w) and x) for the frequency of 0.75 Hz.

The anomaly maps over the full acquisition grid show that the strongest responses occur at 2 Hz, highlighting the plume's evolution across stages. In Model 1, the symmetry of the plume relative to the y-axis results in a symmetrical anomaly, more evident in the Ey field due to the plume's growth direction and the model's anisotropy. In contrast, Model 2, with an asymmetrical plume, presents an asymmetrical anomaly more pronounced in the Ex field, demonstrating how plume geometry influences the electric field response.

Conclusions

This study confirmed the effectiveness of the MCSEM method for monitoring CO_2 plumes in anisotropic media. Using vector finite elements, it was possible to accurately simulate the electromagnetic response, showing that plume geometry and anisotropy directly influence the measured fields. Model 1 showed clearer anomalies in Ey (symmetry), while Model 2 stood out in Ex (lateral asymmetry). The frequency of 2 Hz was the most efficient for visualizing the anomalies. As a follow-up, we suggest simulating scenarios with noise and using anisotropic 3D inversion to better represent the spatial evolution of the plumes over time.

References

Fawad, M., and N. H. Mondol, 2021, Monitoring geological storage of co2: A new approach: Scientific Reports, **11**, 5942.

Kang, S., K. Noh, S. J. Seol, and J. Byun, 2015, mcsem inversion for co2 sequestration monitoring at a deep brine aquifer in a shallow sea: Exploration Geophysics, **46**, 236–252.

REZENDE, D. P., et al., 2011, Análise da componente magnética em dados mcsem 1d.

Soeder, D. J., 2021, Greenhouse gas sources and mitigation strategies from a geosciences perspective: Advances in Geo-Energy Research, **5**, 274–285.

SOUZA, V. C. T. d., et al., 2007, Modelagem numérica de dados mcsem 3d usando computação paralela.

Wang, F., J. P. Morten, and K. Spitzer, 2018, Anisotropic three-dimensional inversion of csem data using finite-element techniques on unstructured grids: Geophysical Journal International, **213**, 1056–1072.

Xiong, B., Y. Lu, H. Chen, Z. Cheng, H. Liu, and Y. Han, 2023, A new 3d marine controlled-source electromagnetic modeling algorithm based on two new types of quadratic edge elements: Applied Sciences, **13**, 2821.

Zhang, L., W. Nowak, S. Oladyshkin, Y. Wang, and J. Cai, 2023, Opportunities and challenges in co2 geologic utilization and storage: Advances in Geo-Energy Research, **8**, 141–145.